Multistability of Driven-Dissipative Quantum Spins

Haggai Landa,[1,*] Marco Schiró,[1,†] and Grégoire Misguich[1,2,‡]

[1] *Institut de Physique Théorique, Université Paris-Saclay, CEA, CNRS, 91191 Gif-sur-Yvette, France*
[2] *Laboratoire de Physique Théorique et Modélisation, CNRS UMR 8089, Université de Cergy-Pontoise, 95302 Cergy-Pontoise, France*

We study the dynamics of coupled quantum spins one-half on a lattice with nearest-neighbour "XY" (flip-flop) interactions, driven by external fields and subject to dissipation. The meanfield limit of the model manifests bistable parameter regions of two coexisting steady states with different magnetizations. We introduce an efficient scheme accounting for the corrections to meanfield by correlations at leading order, and benchmark this scheme using high-precision numerics based on matrix-product-operators in one- and two-dimensional lattices. Correlations are shown to wash the meanfield bistability in dimension one, leading to a unique steady state. In dimension two and higher, we find that multistability is again possible in the thermodynamic limit. It is accompanied by jumps between the different steady states, each showing a critical slowing down in the convergence of perturbations towards the steady state. Experiments with trapped ions can realize the model and possibly answer open questions in the nonequilibrium many-body dynamics of these quantum systems, beyond the system sizes accessible to present numerics.

The level of coherent control over quantum single- and few-body dynamics is continuously improving, spanning atomic, optical, and solid-state systems [1–3]. A major ongoing effort is focused on assembling a large number of such individualy tunable systems and studying the ensuing many-body dynamics. The most significant challenge lies in realizing unitary, closed-system dynamics. However, the inevitable presence of dissipative processes can be utilized in different scenarios, such as in the context of reservoir engineering ideas [4]. Coherent time-periodic driving proves to be a further fruitful tool [5], and a rich pattern of behaviors at the interface between quantum optics and condensed matter physics is observed with systems of strong light-matter interactions [6–22]. Systems characterized by a competition between interactions, nonlinearity, coherent external driving and dissipative dynamics include arrays of coupled Circuit QED (CQED) units [23, 24], cold trapped atoms [25] and ions [26]. Critical phenomena and dissipative phase transitions in these open systems often come with genuinely new properties and novel dynamic universality classes [27–32].

The state of an open quantum system is defined by a density matrix ρ, with the dynamics often treated using a quantum master equation of Lindblad type. It describes a memory-less bath, where the (Markovian) time evolution is generated by the Liouvillian superoperator that acts on ρ [33]. The theoretical tools available for such open quantum many body systems are relatively limited. For driven-dissipative quantum lattice models the meanfield (MF) approach is often employed, and amounts to approximate ρ by a product of single-site density matrices. The resulting dynamics for local observables are described by nonlinear equations, studied, e.g., for lattice Rydberg atoms [34–36], coupled quantum-electrodynamics cavities and circuits [20, 37, 38], nonlinear photonic models [39, 40], and spin lattices [41, 42]. A key property of the MF phase diagrams obtained in those models is that they manifest bistable or multistable parameter regions where two or more steady states are predicted to coexist.

However, the Lindblad equation converges in general to a unique steady state in finite systems [43, 44], making the status of the MF approximation unclear. Indeed, significant deviations from MF have been found using approximation schemes accounting for quantum correlations [45–47], and also using exact numerical methods (quantum trajectories [48] and Matrix Product Operators (MPO) [49]). In one-dimensional (1D) lattices with nearest-neighbour (NN) interactions, the MF bistability is found to be replaced by a crossover driven by large quantum fluctuations [39, 45, 50, 51]. In contrast, in certain 2D NN models, MF bistability has been found by approximate methods to be replaced by a first-order phase-transition between two states, for nonlinear bosons using a truncated Wigner approximation [39, 51], and for Ising spins using a variational ansatz acounting for nearest-neighbors correlations [45], a cluster mean field approach [52] and two-dimensional tensor network states [53]. In a parameter region around the jump, the convergence towards the steady state was found to slow down [45, 51], a phenomenon related to the closing of the gap in the spectrum of the Liouvillian superoperator [54].

In this Letter we study a driven-dissipative model of one-half spins with XY (flip-flop) interactions, which is also the limit of a driven-dissipative Bose-Hubbard model at large nonlinearity and small boson occupancy. We introduce an approximation scheme based on the coupling of the MF to Quantum Fluctuations (MFQF), accounting for the modification of the MF dynamics due to the feedback of correlations in the leading order. In combination with MPO simulations we show that this approximation captures the large quantum fluctuations that wash

* haggaila@gmail.com
† marco.schiro@ipht.fr
‡ gregoire.misguich@cea.fr

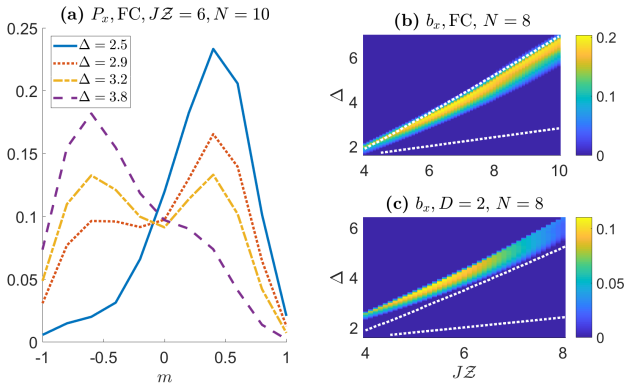

FIG. 1. (a) Probability distribution $P_x = P(M_x = m)$ of the x magnetization per-site ($M_x = \frac{1}{N}\sum_R \sigma_R^x$), for a few values of the detuning Δ, at fixed $J\mathcal{Z}$ and $\Omega = 0.5$, in the steady state of Eqs. (1)-(3) with $N = 10$ spins on a fully connected (FC) lattice. The transition from a single peak centered at $m > 0$ (low Δ) to a single peak at $m < 0$ as Δ is increased, is accompanied by an intermediate region of a bimodal distribution. (b) The bimodality index b_x (see text) given by the color code as a function of Δ and $J\mathcal{Z}$, with $\Omega = 0.5$ and $N = 8$ for the FC lattice. Within the region bounded by the two white dotted lines, the meanfield limit manifests bistability of two different steady-state magnetizations $\mu_a^S = \lim_{t\to\infty}\langle M_a\rangle$. (c) b_x for a two-dimensional ($2D$) parallelogram of $N = 8$ sites and periodic boundary conditions (note the smaller $J\mathcal{Z}$ range). We find bimodality again, although weaker than in the FC model, and with stronger finite-size effects.

the MF bistability in 1D, confirming the existence of a unique steady state in the thermodynamic limit. As our main result, we find that in dimension two and higher multistability is again possible, with jumps between the different steady states, accompanied by a critical slowing down.

Model. We consider an open quantum system with N sites $R \in \mathbb{Z}^D$ on a hyper-cubic lattice in D spatial dimensions, for which the connectivity is $\mathcal{Z} = 2D$. Additionally, we consider a fully-connected (FC) model, i.e. a graph where all sites are linked (whence $\mathcal{Z} = N - 1$). The master equation for the density matrix ρ in the Schrödinger picture is

$$\partial_t \rho = -i[H, \rho] + \mathcal{D}[\rho], \qquad \hbar = 1. \tag{1}$$

The Hamiltonian describing Rabi oscillations of two-level systems with a drive detuned by Δ from the resonant transition frequency and a Rabi frequency Ω, is given in a frame rotating with the drive by

$$H = \sum_R \left[\frac{\Delta}{2}\sigma_R^z + \Omega\sigma_R^x\right] - \sum_{\langle R,R'\rangle} J\left(\sigma_R^+\sigma_{R'}^- + \text{h.c.}\right), \tag{2}$$

where the second sum extends over all pairs of NN sites, describing hopping with amplitude J, with spin-$\frac{1}{2}$ operators (Pauli matrices) σ_R^a, $a = \{x, y, z\}$, and $\sigma_R^\pm = (\sigma_R^x \pm i\sigma_R^y)/2$. The Lindblad dissipator for spin losses occurring independently at each site with rate $\Gamma = 1$ (which sets the frequency and time units), is

$$\mathcal{D}[\rho] = \sum_R \left[\sigma_R^-\rho\sigma_R^+ - \frac{1}{2}\left(\sigma_R^+\sigma_R^-\rho + \rho\sigma_R^+\sigma_R^-\right)\right]. \tag{3}$$

Aside from translation invariance, this model has no manifest symmetries. The meanfield phase diagram of this model is known to display bistability [42, 50], while in 1D a unique steady state has been found using MPO simulations [50]. Here we focus on higher dimensions, which we find to manifest bistability in the thermodynamic limit.

Precursors of Bistability in Finite size systems. We first solve the dynamics exactly for small FC clusters (up to $N = 10$). As the thermodynamic limit $N \to \infty$ is approached in the FC lattice, the MF bistability is expected to be regained [55]. A picture that allows to reconcile the MF behavior in the $N = \infty$ limit with the fact that for any finite N the system must have a unique steady state, is that of a state where observables are distributed in a bimodal way, with peaks located close to the two MF steady-state values, and becoming sharper and narrower as N increases. Figure 1(a) shows a few curves of the probability distribution of the x magnetization per site, i.e. $P_x = P(M_x = m)$, where $M_x = \frac{1}{N}\sum_R \sigma_R^x$. At fixed Ω and $J\mathcal{Z}$ (the rescaling by $\mathcal{Z}$ allows to compare lattices of a different connectivity), a variation of Δ leads to P_x changing from a single peak centered about $m > 0$ to a single peak centered about $m < 0$, with an intermediate Δ range where P_x has two separated peaks. To quantify the bimodality of the distribution we define an index $b_x = 2(P_{\max,2} - P_{\min})/(P_{\max,1} + P_{\max,2})$, where $P_{\max,2} \le P_{\max,1}$ are the two maxima of the distribution, and $P_{\min}$ is the minimum between the two. As can be seen in Fig. 1(b), the extent of the bimodality region in Δ and the maximum of b_x increase with $J\mathcal{Z}$ at a fixed Ω, following the MF bistability region (described below). We note that another precursor of bistability in small lattices is the decrease of the Liouvillian gap in the MF bistability region [42].

We now repeat this analysis in finite dimension: a 1D chain with periodic boundary conditions (BC), and a 2D square lattice with periodic BC. We find (not shown) that b_x remains strictly zero for a 1D chain (with $N = 8$) for the same parameters as in Fig. 1(b), while in 2D we find that $b_x > 0$ in a whole region in the parameter plane, see Fig. 1(c). With an increasing interaction strength J, the magnitude and extent of correlated fluctuations in the lattice grow, which explains the gradual decrease of the parameter region where bimodality is observed for a small lattice. The region and the maximum b_x obtained in 2D are smaller than in the FC model and also shifted towards higher Δ (as in much larger lattices shown below). As a further consistency check, we verified that when increasing N (up to 10) at specific parameter values, the bimodality range and maximum increase (see App. A). To make further progress, we turn to study larger systems.

MPO Calculations. The density matrix ρ can be considered as a pure state in an enlarged Hilbert space with four states per site [56]. This approach allows one to solve the Lindblad evolution using a method that is formally similar to the unitary evolution of a pure state encoded using well-established matrix product states (see [57, 58] and references therein). We numerically solve for the dynamics of ρ in a 1D chain with open BC using an MPO algorithm [49, 56, 59], with an implementation based on the iTensor library [60], and a Trotter decomposition of order four [58, 61]. The number of spins was varied up to 200, and we checked that observables measured in the central region of the chain had negligible finite-size effects. As for the MPO bond dimension, the data shown here were obtained with $\chi = 300$, insuring that truncation errors are negligible at the scale of the plots, thus providing some benchmark for the MFQF method.

Dynamics of Observables. From the master equation one can also derive a hierarchy of equations of motion for n-points expectation values of the form $\langle \sigma^a_{R_1} \sigma^b_{R_2} \cdots \sigma^c_{R_n} \rangle \equiv \mathrm{tr}\{\rho \sigma^a_{R_1} \sigma^b_{R_2} \cdots \sigma^c_{R_n}\}$, which depend on the value of correlators at the next order $n+1$. Assuming that the density matrix is translationally-invariant and remains so during the time evolution, we define the vector mean magnetization (uniform over the sites), $\mu_a(t) = \langle M_a \rangle = \langle \sigma^a_R \rangle$, with its equations of motion

$$\partial_t \mu_x = -J\mathcal{Z}[\mu_y \mu_z + \eta_{yz}(1)] - \Delta \mu_y - \mu_x/2, \quad (4)$$

$$\partial_t \mu_y = J\mathcal{Z}[\mu_x \mu_z + \eta_{xz}(1)] - 2\Omega \mu_z + \Delta \mu_x - \mu_y/2, \quad (5)$$

$$\partial_t \mu_z = 2\Omega \mu_y - (1 + \mu_z)\,. \quad (6)$$

Here, we have defined the connected two-point correlation functions,

$$\eta_{ab}(R, R', t) \equiv \left\langle \left(\sigma^a_R - \mu_a\right)\left(\sigma^b_{R'} - \mu_b\right)\right\rangle = \left\langle \sigma^a_R \sigma^b_{R'} \right\rangle - \mu_a \mu_b, \quad R \neq R', \quad (7)$$

and setting $R' = 0$ using the translation invariance, $\eta_{ab}(1)$ is the correlator at a NN of the origin.

Equations (4)-(6) are exact (assuming translation-invariance), involving no approximation as yet. The limit $\eta \to 0$ which amounts to assuming that the density matrix is a product of identical on-site states, leads to the MF equations, whose steady state and dynamics are studied in detail in [62]. We present an approximate scheme to go beyond MF, formally based on an expansion in the inverse of the lattice connectivity (with a related approach in [46]). Neglecting the connected three-point correlators $\left\langle \left(\sigma^a_R - \mu_a\right)\left(\sigma^b_{R'} - \mu_b\right)\left(\sigma^c_{R''} - \mu_c\right)\right\rangle \approx 0$, allows us to derive (see App. D) coupled equations for $\eta_{ab}(R, t)$, which we solve numerically together with their feedback into Eqs. (4)-(6). Since the short-range correlators $\eta_{ab}(1)$ appearing in Eqs. (4)-(6) are dynamically coupled to all distances in the lattice, the MFQF method can account for the spatial structure of correlation functions. The present simulations have been verified to be converged as a function of N and t.

Figure 2(a) shows the x component of the steady-state magnetization, $\vec{\mu}^S \equiv \lim_{t\to\infty} \vec{\mu}(t)$, in 1D, for $J\mathcal{Z} = 4$ as a function of Δ. In MF, $\vec{\mu}^S$ is unique except for $1.3 \lesssim \Delta \lesssim 1.9$, where there are two co-existing stable solutions in addition to an unstable solution. At the presence of quantum correlations, the magnetization departs significantly from the MF prediction (as seen in the curves of MPO and MFQF), with a crossover between the two limiting regimes, in the range $1.5 \lesssim \Delta \lesssim 5$. We define the inverse correlation lengths λ_{ab} by fitting the six correlation functions $\eta_{ab}(R)$ to $\eta_{ab}(R) \sim \exp\{-\lambda_{ab} R\}$. For simplicity, we present in Fig. 2(b) only one correlation length, and Fig. 2(c) shows the corresponding total correlation measured by $\Sigma_{ab} = \sum_R \eta_{ab}(R)$. From the combination of the two we deduce that the spatial structure of the two-point correlation undergoes a sharp change within the crossover region, from relatively small but widely extended correlations for low Δ, to much larger but very short-ranged correlations, for high Δ. A detailed analysis of the correlations shows that at the same time, the correlations change nature from showing periodical modulations (spin density-wave character), to being overdamped in space.

As Fig. 2 shows, the MFQF approximation correctly captures the uniqueness of the steady state and the disappearance of bistability. On both sides of the crossover

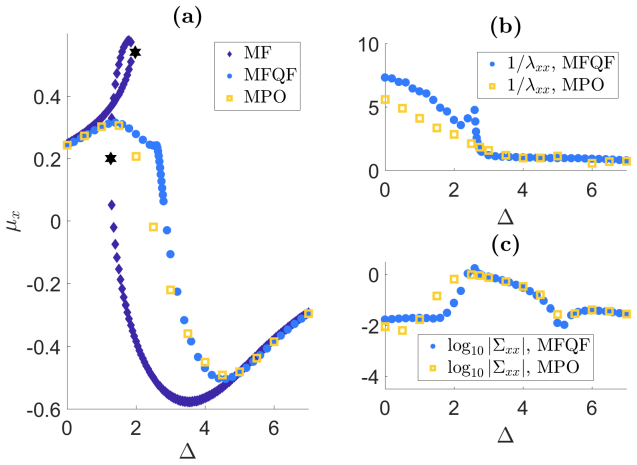

FIG. 2. (a) Mean steady-state x magnetization μ_x^S as a function of Δ for $\Omega = 0.5$ and $J\mathcal{Z} = 4$, on a 1D lattice. The mean-field (MF) limit manifests bistability, with three co-existing solutions, two of which – those on the branches coming from the limits of $\Delta \to \{0, \infty\}$, are stable. Two black hexagrams mark the points where the unstable branch meets each of the two stable ones. An exact numerical treatment using Matrix Product Operators (MPO) shows a crossover within a range of Δ shifted from the MF bistability region. An approximation incorporating quantum fluctuations at leading order (MFQF) follows approximately the MPO result in a large range of parameters. (b) The correlation length λ_{xx} defined by fitting $\eta_{xx} \sim \exp\{-\lambda_{xx} R\}$, and (c) the total correlation $\Sigma_{xx} = \sum_R \eta_{xx}(R)$, calculated in MPO and MFQF, showing that the latter approximation is capable of capturing the spatial structure and relative magnitudes of two-point correlations in the lattice, which lead to significant deviations from the MF decoupling limit.

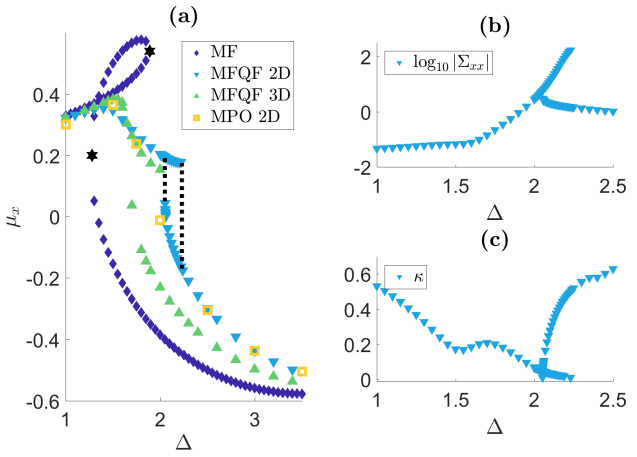

FIG. 3. (a) Mean steady-state x magnetization μ_x^S in the MFQF approximation in 2D-3D, together with the MF limit and 2D-MPO results (for a finite-size, 12×4 cylinder). The parameters are as in Fig. 2, with $J\mathcal{Z}$ kept fixed by varying J with the dimension. In contrast to the 1D case, for $D \geq 2$ MFQF predicts multistability, with two stable branches progressively converging towards the meanfield branches in an increasingly larger parameter region. The dotted black lines indicate the edges of the 2D bistable region. The simulations were run with lattices of up to 200^2 and 40^3 sites and periodic BC. (b) The total correlation in 2D, showing a difference of up to two orders of magnitude in the bistable phases. (c) The rate of convergence to the steady state, fitted to an exponential form $\sim e^{-\kappa t}$, showing a critical slowing down of the decay dynamics as $\kappa \to 0$ at the two edges of the bistable branches.

region, the results are quantitatively accurate. In its center, the approximation reaches large values for $\eta_{ab}(R)$ and the correlation length, and is only qualitatively correct. More generally, we find that as J is increased in 1D, the MFQF approach loses its accuracy (within the parameter region of strong correlations), plausibly because of the role of higher-order correlation functions that are neglected, which can lead at much larger J to the break down of the approximation. However, the MFQF approach is easy to generalize to higher dimensions, and quantitatively accurate in regions with moderate correlations.

Higher dimensions. Figure 3(a) shows the results of simulations with large 2D and 3D lattices, for $J\mathcal{Z} = 4$. The MFQF theory is compared with 2D-MPO calculations, where, as in 1D, the time-dependent many-body density matrix is encoded as a product of matrices. The matrix product runs over a snake-like path visiting all the sites of a cylinder of length $L_x = 12$ and perimeter $L_y = 4$ (see App. C). Such an approach has been successfully applied in ground-state calculations of 2D models [63], but we are not aware of previous 2D-MPO calculations in the Lindblad framework. For $\Delta \lesssim 1.5$ and $\Delta \gtrsim 2.5$ the agreement between MPO and MFQF is almost perfect, giving a nontrivial check of the ability of MFQF to capture significant correlation effects (that result in $\vec{\mu}$ strongly departing from its meanfield value in this regime). The computational cost of guaranteeing a high accuracy in the calculation is exponential in L_y (see App. C), limiting the present MPO calculations to relatively small systems, which cannot show bistability (and a possible discontinuity would also be smeared out by the finite size effects).

Using MFQF, and in contrast to 1D, we find in $D \geq 2$ two stable $\vec{\mu}^S$ branches, in progressively larger ranges of Δ, which converge towards the MF bistability region and the MF magnetization values. This is our main result, and the MFQF framework allows to characterize the dynamics and correlation functions in detail. As an example, Fig. 3(b) shows that Σ_{xx} increases by two orders of magnitude for one of the bistable states, and Fig. 3(c) shows the asymptotic relaxation rate associated to the convergence to $\vec{\mu}^S$. It is obtained by fitting $\partial_t \vec{\mu}^2 \sim e^{-\kappa t}$ at large times ($t \sim 100$). The fact that $\kappa \to 0$ at the branch edges in 2D indicates a critical slowing down when approaching the end of the bistability region in the phase that is about to disappear, leading to a discontinuous jump. The MFQF approach does however not *always* predict bistability in 2D. Indeed, replacing each hopping term in Eq. (2) by the Ising coupling $J_z \sigma_R^z \sigma_{R'}^z$, we find a smooth crossover for moderate values of the interaction (as obtained using cluster mean-field [52]), and a small bistability region for stronger spin-spin couplings (again as in [52]); See App. B for details.

Experimental feasibility. In addition to possible experimental realizations with circuit-QED arrays [50], the present driven-dissipative spin model can be realized in current experiments with a few tens to a few hundreds of trapped ions. XY interactions can be implemented by superposing two laser beams inducing spin-motion coupling along two orthogonal spatial directions [64–66], with an additional laser for the on-site Hamiltonian. As recently demonstrated experimentally, the interaction can be varied from being almost independent of distance to a dipolar power-law, and therefore short-range in 1D [67, 68] and 2D lattices [26]. The interaction strength in these works is of order $J/\hbar \sim 10^4 s^{-1}$, one to two orders of magnitude larger than the qubit dephasing rates, and the rate of spin-flip processes in Eq. (3) can be controlled as well.

Discussion. Studying lattices of driven-dissipative interacting spins using state-of-the-art 1D MPO simulations we have found no phase transition but a crossover between two regimes with different characteristics. On the other hand, a fully-connected graph (for which there is no notion of distance) approaches the meanfield limit in the thermodynamic limit, manifesting bistability and magnetization jumps. Between these two limits, both the lattice dimension and the range of interactions could determine the onset of critical phenomena. Using a new approximate approach that accounts for the leading-order lattice correlations and their feedback into the mean magnetization, we find that bistability is possible in a driven-dissipative quantum systems already in 2D, accompanied by jumps.

Exact diagonalization of small systems suggests that bistability in the thermodynamic limit is obtained through an increasingly sharper bimodality of the probability distribution in finite systems. Although the scaling with N of the bimodal peaks in the exact probability distribution, is beyond the scope of the current work, we emphasize that for N large but finite, long-lived metastable states are expected as precursors of bistability. Their lifetimes diverge with N, plausibly $\propto e^N$, and for large enough N, their timescale greatly exceeds that accessible in numerical or experimental realizations. As a parameter is swept across the bistability region in the two possible senses, observables will show hysteretic loops – unless the sweep is unrealistically slow, *i.e.* $\propto e^{-N}$. At the same time, the finite-size steady state may be schematically viewed as some combination of the two metastable states, and an observable computed by taking first the limit $t \to \infty$ and then $N \to \infty$ will, by construction, be independent of the system history. This steady state observable might in particular be discontinuous at some particular value of the parameter, as argued in different contexts [39, 44, 51, 69]. Hence, a unique steady state with a discontinuous jump is a priori compatible with bistability and hysteresis and, in the present scenario, finding one or the other is a matter of order of limits.

To conclude, the present exact and approximate calculations suggests that $D = 2$ is a lower critical dimension for bistability in this problem. The question of the existence of a lower critical dimension for bistability, bimodality and hysteresis and the accompanied dissipative phase transitions in this model can be directly addressed experimentally. If a definite answer is found, it would constitute the first demonstration of deciding an important question currently intractable classically, obtained using a controlled quantum simulation. It could clarify the status of the meanfield approximation in these systems, and shed light on the fundamental differences between equilibrium and nonequilibrium phase transitions.

ACKNOWLEDGMENTS

We acknowledge the DRF of CEA for providing us with CPU time on the supercomputer COBALT of the CCRT. H.L. thanks Roni Geffen for fruitful discussions, and acknowledges support by IRS-IQUPS of Université Paris-Saclay and by LabEx PALM under grant number ANR-10-LABX-0039-PALM.

Appendix A: Bimodality as a function of lattice size

Figure 4 shows the bimodality index b_x calculated exactly for three increasing lattice sizes (in the 2D case shown in panel (b), different parallelograms are constructed with periodic boundary conditions to incorporate N sites), for the driven-dissipative XY model discussed in the main main text. Although sensitive to the finite system size, the width of the Δ ranges of bimodality increase with N and the maximal b_x value increases accordingly, which is consistent with bistability in the $N \to \infty$ limit.

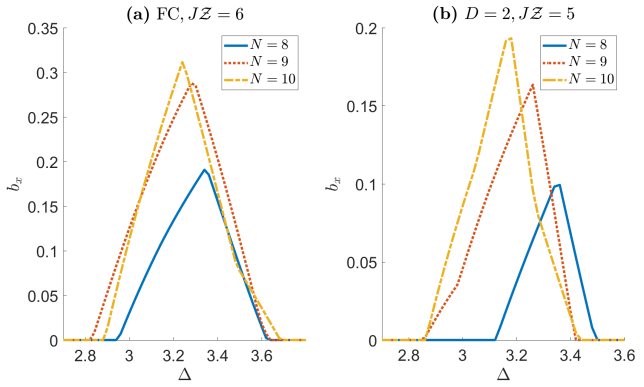

FIG. 4. The bimodality index b_x (see text) as a function of Δ for (a) $J\mathcal{Z} = 6$ in a fully-connected (FC) lattice, and (b) $J\mathcal{Z} = 5$ in a 2D lattice, from exact numerical solutions of the master equation of the driven-dissipative XY model, for small lattices, with three values of $N = 8, 9, 10$.

Appendix B: Bistability in a driven-dissipative Ising model in 2D

We have employed the MFQF method to the study of the driven dissipative Ising model, obtained after replacing the XY (flip-flop) interaction term in the Hamiltonian,

$$H = \sum_R \left[\frac{\Delta}{2}\sigma_R^z + \Omega\sigma_R^x\right] - \sum_{\langle R,R'\rangle} \frac{J_z}{2}\sigma_R^z\sigma_{R'}^z, \qquad \text{(B1)}$$

while keeping the dissipator identical. The equations of motion for $\vec{\mu}$ that are obtained from this model are identical to those in Eqs. (4)-(6) of the main text with just the replacement $J \to -J_z$. The correlator equations (given in the following), are different.

Setting $\Delta = 0$ we have studied the resulting MFQF steady state on a 2D lattice. A necessary condition for bistability in the meanfield limit [62], is $|J_z\mathcal{Z}| > 2$. For $J_z\mathcal{Z} = -4$, Fig. 5 shows a smooth crossover of the steady-state magnetization $\vec{\mu}^S$ as a function of Ω across the parameter region of meanfield bistability. The z magnetization curve of Fig. 5(b) can be compared with the results plotted in Fig. 1(a) of [52], which were obtained using a cluster MF approach for different cluster sizes. In the notation of Ref. [52], $J_z\mathcal{Z} = -V/\gamma$ and $\Omega = (h_x/\gamma)/2$, making the parameters in the plots identical (with only a somewhat larger range taken here for the abscissa). The MFQF curve that we obtain contains a further noticeable feature around $\Omega \approx 1.5$, with a relatively sharper change in magnetization.

In Fig. 6, μ_x^S and μ_z^S are shown for $J_z\mathcal{Z} = -6$, in a larger region of Ω across the parameter region of mean-

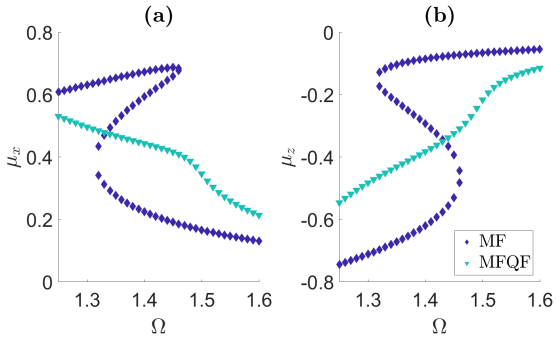

FIG. 5. (a) Mean steady-state x magnetization μ_x^S as a function of Ω for $\Delta = 0$ and $J_z\mathcal{Z} = -4$, on a 2D lattice for the Ising model. (b) The mean steady-state z magnetization for the same parameters. The MF manifests bistability in the Ω range shown, while MFQF predicts a smooth crossover. We note that in the notation of Ref. [52], $\Omega = (h_x/\gamma)/2$, and $J_z\mathcal{Z} = -V/\gamma$ and the current figure corresponds to Fig. 1(a) of Ref. [52], in a somewhat larger Ω range, showing a rather sharp change around $\Omega \approx 1.5$. The simulation accounts for a lattice of 100^2 sites, and the results have been verified to converge in N and t.

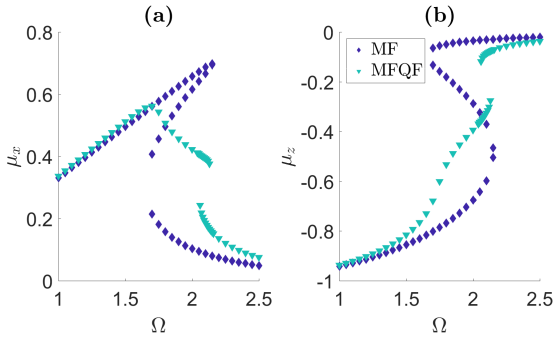

FIG. 6. (a) Mean steady-state x magnetization μ_x^S as a function of Ω for $\Delta = 0$ and $J_z\mathcal{Z} = -6$, on a 2D lattice for the Ising model. (b) The mean steady-state z magnetization for the same parameters. The MF manifests bistability in the large Ω range shown, while MFQF predicts a shrinking of the bostability region and its occurrence at the edge of the Ω range. We note that in the notation of Ref. [52], $\Omega = (h_x/\gamma)/2$, and $J_z\mathcal{Z} = -V/\gamma$ and the current figure corresponds to Fig. 1(b) of Ref. [52]. The simulation accounts for a lattice of 100^2 sites, and the results have been verified to converge in N and t. See Fig. 7 for the characteristics of corrleation functions around the bistable region.

field bistability. The z magnetization curve of Fig. 6(b) can be compared with the curves plotted in Fig. 1(b) of [52]. In the region where the cluster MF of Ref. [52] predicts a shrinking of the bistability (but not its complete disappearance up to the largest available cluster size), MFQF predicts a rather sharp but smooth crossover. However in MFQF approach bistability remains in a small region ($2.06 \lesssim \Omega \lesssim 2.13$), at the right edge of MF bistability region. The structure of these the two coexisting stable phases is distinctly different in terms of

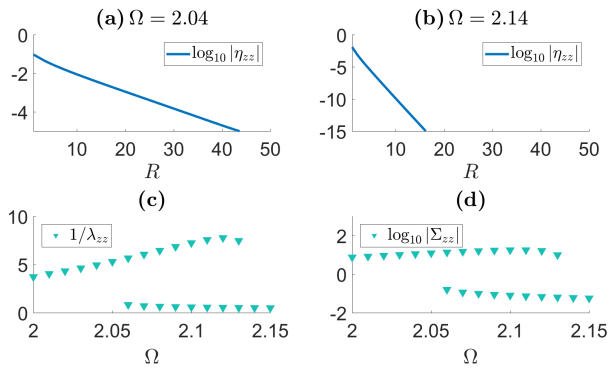

FIG. 7. Characteristics of the correlation functions around the bistable region of Fig. 6. (a)-(b) The correlation function $\eta_{zz}(R)$ as a function of the distance for two different Ω values (outside the bistability region). Note the different scales of the two plots. (c) The correlation length (along one spatial direction) as a function of Ω, showing a difference of up to an order of magnitude in the bistable phases. (d) The total correlation $\Sigma_{zz} = \sum_R \eta_{zz}$, showing a difference of up to two orders of magnitude in the bistable phases.

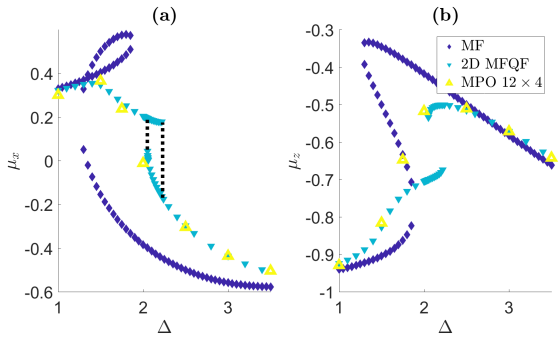

FIG. 8. (a) Mean steady-state x magnetization μ_x^S and (b) z magnetization μ_z^S, in the MFQF approximation in 2D, together with the MF limit and 2D-MPO results (for a finite-size, 12×4 cylinder). The parameters are as in Fig. 3 of the main text.

the correlation functions $\eta_{ab}(R)$ defined in Eq. (7) of the main text. Figure 7 presents the characteristics of $\eta_{zz}(R)$ as an example, showing the large differences in the correlation length, and – as a result – the total correlation, between the two bistable states.

Appendix C: 2D-MPO

The 2D MPO calculations presented in Fig. 3 of the main text and in Fig. 8, have been carried out on cylinders of length L_x from 8 to 16, and fixed $L_y = 4$. At fixed precision the required bond dimension χ is expected to be constant with L_x, but exponentially large in L_y. The data is obtained with a bond dimension $\chi = 400$ (pushed to $\chi = 600$ at $\Delta = 1.75$). As in the 1D-MPO result, the steady state is obtained by evolving ρ in time from an

initial state where all the spins are pointing down. In practice a total time between 15 and 25 was used. Since the path of interacting spins associated to the MPO artificially breaks the translation invariance of the lattice in the y direction, it is important to check that the bond dimension is large enough to restore the translation symmetry in the observables. In our case the magnetization was found to be translation invariant up to relative errors of the order of $\mathcal{O}(10^{-4})$.

Appendix D: Meanfield with Quantum Fluctuations

To derive the equations of the MFQF approach, we define a two-point correlation function (correlator),

$$\vartheta_{ab}(R,R',t) \equiv \left\langle \sigma^a_R \sigma^b_{R'} \right\rangle, \qquad R \neq R', \tag{D1}$$

which is a function of the difference $R - R'$ alone, symmetric in a, b (because $\sigma^a_{R'}$ and σ^b_R commute). Using Eq. (D1), the connected two-point correlator is defined as in Eq. (7) of the main text, for $R \neq R'$, by

$$\eta_{ab}(R,R',t) = \vartheta_{ab}(R,R') - \mu_a \mu_b, \tag{D2}$$

The connected three-point correlator is defined for $R \neq R' \neq R''$ by

$$\zeta_{abc}(R,R',R'',t) \equiv \left\langle (\sigma^a_R - \mu_a)\left(\sigma^b_{R'} - \mu_b\right)(\sigma^c_{R''} - \mu_c) \right\rangle, \tag{D3}$$

which is again a function of the differences only.

The approximation of the following treatment is based on assuming that ζ (and higher order connected correlators) can be neglected in comparison to η. The e.o.m of ϑ_{ab}, setting $R' = 0$, is

$$\partial_t \vartheta_{ab}(R) = \sum_d \Pi_{ad}\vartheta_{db}(R) + \sum_d \Pi_{bd}\vartheta_{ad}(R) + f_{ab}(\mu,\vartheta) + g_{ab}(\mu,\vartheta), \tag{D4}$$

where the local Hamiltonian terms are described using the matrix

$$\Pi = \begin{pmatrix} 0 & -\Delta & 0 \\ \Delta & 0 & -2\Omega \\ 0 & 2\Omega & 0 \end{pmatrix}, \tag{D5}$$

while $f_{ab}(\mu,\vartheta) \propto J$ comes from the kinetic terms, and $g_{ab}(\mu,\vartheta) \propto \Gamma$ comes from the Lindbladian part, and both are given below. By using Eq. (D2) we get the e.o.m system for $\eta(R,t)$,

$$\partial_t \eta_{ab}(R,t) = \partial_t \vartheta_{ab}(R) - \partial_t \left[\mu_a \mu_b\right], \tag{D6}$$

which we solve numerically together with the coupled system for $\vec{\mu}(t)$.

For the Hamiltonian in Eq. (2) of the main text where the kinetic term is

$$-\sum_{\langle R,R'\rangle} J\left(\sigma^+_R \sigma^-_{R'} + \text{h.c.}\right) = -\sum_{\langle R,R'\rangle} \frac{J}{2}\left(\sigma^x_R \sigma^x_{R'} + \sigma^y_R \sigma^y_{R'}\right), \tag{D7}$$

we find that $f_{ab}(\mu,\vartheta)$ of Eq. (D4) is given by,

$$f_{xx}(R) = 2J\left[2\mu_x\mu_y\mu_z - \mu_x\vartheta_{yz}(1) - \mu_y\vartheta_{xz}(R)\right]\left[\mathcal{Z} - \delta_{\|R\|,1}\right] - 2J \sum_{\substack{R'\neq 0 \\ \|R'-R\|=1}} \mu_z \vartheta_{xy}(R'), \tag{D8}$$

$$f_{yy}(R) = -2J\left[2\mu_x\mu_y\mu_z - \mu_y\vartheta_{xz}(1) - \mu_x\vartheta_{yz}(R)\right]\left[\mathcal{Z} - \delta_{\|R\|,1}\right] + 2J \sum_{\substack{R'\neq 0 \\ \|R'-R\|=1}} \mu_z \vartheta_{xy}(R'), \tag{D9}$$

$$f_{zz}(R) = -2J\left[\mu_x\vartheta_{yz}(R) - \mu_y\vartheta_{xz}(R)\right]\left[\mathcal{Z} - \delta_{\|R\|,1}\right] - 2J \sum_{\substack{R'\neq 0 \\ \|R'-R\|=1}} \left[\mu_y\vartheta_{xz}(R') - \mu_x\vartheta_{yz}(R')\right]. \tag{D10}$$

$$f_{xy}(R) = J\left[2\mu_y^2\mu_z - 2\mu_x^2\mu_z - \mu_y\vartheta_{yz}(1) - \mu_y\vartheta_{yz}(R) + \mu_x\vartheta_{xz}(1) + \mu_x\vartheta_{xz}(R)\right]\left[\mathcal{Z} - \delta_{\|R\|,1}\right] - J \sum_{\substack{R'\neq 0 \\ \|R'-R\|=1}} \left[\mu_z\vartheta_{yy}(R') - \mu_z\vartheta_{xx}(R')\right], \tag{D11}$$

$$f_{xz}(R) = -J\mu_y\delta_{\|R\|,1} + J\left[2\mu_z^2\mu_y - \mu_z\vartheta_{yz}(1) - \mu_y\vartheta_{zz}(R) - \mu_x\vartheta_{xy}(R) + \mu_y\vartheta_{xx}(R)\right]\left[\mathcal{Z} - \delta_{\|R\|,1}\right] - J\sum_{\substack{R'\neq 0\\ \|R'-R\|=1}}\left[\mu_z\vartheta_{yz}(R') + \mu_y\vartheta_{xx}(R') - \mu_x\vartheta_{xy}(R')\right], \quad \text{(D12)}$$

$$f_{yz}(R) = J\mu_x\delta_{\|R\|,1} + J\left[-2\mu_z^2\mu_x + \mu_z\vartheta_{xz}(1) + \mu_x\vartheta_{zz}(R) - \mu_x\vartheta_{yy}(R) + \mu_y\vartheta_{xy}(R)\right]\left[\mathcal{Z} - \delta_{\|R\|,1}\right] + J\sum_{\substack{R'\neq 0\\ \|R'-R\|=1}}\left[\mu_z\vartheta_{xz}(R') - \mu_y\vartheta_{xy}(R') + \mu_x\vartheta_{yy}(R')\right]. \quad \text{(D13)}$$

The components of $g(\mu,\vartheta)$ in Eq. (D4) are given by

$$g_{aa} = -\Gamma\vartheta_{aa}, \quad g_{xy} = -\Gamma\vartheta_{xy}, \quad g_{xz} = -\Gamma\left[2\vartheta_{xz} + \frac{3}{2}\mu_x\right], \quad g_{yz} = -\Gamma\left[2\vartheta_{yz} + \frac{3}{2}\mu_y\right]. \quad \text{(D14)}$$

For the Ising model of Eq. (B1) where the kinetic term is

$$-\sum_{\langle R,R'\rangle}\frac{J_z}{2}\sigma_R^z\sigma_{R'}^z, \quad \text{(D15)}$$

we get instead of the above $f_{ab}(\mu,\vartheta)$, the following expressions;

$$f_{xx}(R) = -2J_z\left[2\mu_x\mu_y\mu_z - \mu_x\vartheta_{yz}(1) - \mu_z\vartheta_{xy}(R)\right]\left[\mathcal{Z} - \delta_{\|R\|,1}\right] + 2J_z\sum_{\substack{R'\neq 0\\ \|R'-R\|=1}}\mu_y\vartheta_{xz}(R'), \quad \text{(D16)}$$

$$f_{yy}(R) = 2J_z\left[2\mu_x\mu_y\mu_z - \mu_y\vartheta_{xz}(1) - \mu_z\vartheta_{xy}(R)\right]\left[\mathcal{Z} - \delta_{\|R\|,1}\right] - 2J_z\sum_{\substack{R'\neq 0\\ \|R'-R\|=1}}\mu_x\vartheta_{yz}(R'), \quad \text{(D17)}$$

$$f_{zz}(R) = 0. \quad \text{(D18)}$$

$$f_{xy}(R) = J_z\left[2\mu_x^2\mu_z - 2\mu_y^2\mu_z - \mu_x\vartheta_{xz}(1) - \mu_z\vartheta_{xx}(R) + \mu_y\vartheta_{yz}(1) + \mu_z\vartheta_{yy}(R)\right]\left[\mathcal{Z} - \delta_{\|R\|,1}\right] + J_z\sum_{\substack{R'\neq 0\\ \|R'-R\|=1}}\left[\mu_y\vartheta_{yz}(R') - \mu_x\vartheta_{xz}(R')\right], \quad \text{(D19)}$$

$$f_{xz}(R) = J_z\mu_y\delta_{\|R\|,1} - J_z\left[2\mu_z^2\mu_y - \mu_z\vartheta_{yz}(1) - \mu_z\vartheta_{yz}(R)\right]\left[\mathcal{Z} - \delta_{\|R\|,1}\right] + J_z\sum_{\substack{R'\neq 0\\ \|R'-R\|=1}}\mu_y\vartheta_{zz}(R'), \quad \text{(D20)}$$

$$f_{yz}(R) = -J_z\mu_x\delta_{\|R\|,1} + J_z\left[2\mu_z^2\mu_x - \mu_z\vartheta_{xz}(1) - \mu_z\vartheta_{xz}(R)\right]\left[\mathcal{Z} - \delta_{\|R\|,1}\right] - J_z\sum_{\substack{R'\neq 0\\ \|R'-R\|=1}}\mu_x\vartheta_{zz}(R'). \quad \text{(D21)}$$

[1] S. Haroche and J. Raimond, *Exploring the Quantum: Atoms, Cavities, and Photons*, 1st ed. (Oxford University Press, USA, 2006).

[2] Y. Yamamoto, F. Tassone, and H. Cao, *Semiconductor Cavity Quantum Electrodynamics*, 1st ed. (Springer, 2000).

[3] R. J. Schoelkopf and S. M. Girvin, Nature **451**, 664 (2008).

[4] C. Bardyn, M. Baranov, C. Kraus, E. Rico, A. İmamoğlu, P. Zoller, and S. Diehl, New Journal of Physics **15**, 085001 (2013).

[5] T. Oka and S. Kitamura, Annual Review of Condensed Matter Physics **10**, null (2019), https://doi.org/10.1146/annurev-conmatphys-031218-013423.

[6] A. D. Greentree, C. Tahan, J. H. Cole, and L. C. L. Hollenberg, Nature Physics **2**, 856 (2006).

[7] M. Hartmann, F. Brandao, and M. B. Plenio, Nature Physics **2**, 849 (2006).

[8] D. E. Chang, V. Gritsev, G. Morigi, V. Vuletic, M. D. Lukin, and E. A. Demler, Nature Physics **4**, 884 (2008).

[9] J. Koch, A. A. Houck, K. L. Hur, and S. M. Girvin, Phys. Rev. A **82**, 043811 (2010).

[10] A. Petrescu, A. A. Houck, and K. Le Hur, Phys. Rev. A **86**, 053804 (2012).

[11] J. Cho, D. G. Angelakis, and S. Bose, Phys. Rev. Lett. **101**, 246809 (2008).

[12] R. O. Umucallar and I. Carusotto, Physical Review A **84**, 043804 (2011).

[13] M. Hafezi, M. D. Lukin, and J. M. Taylor, New Journal of Physics **15**, 063001 (2013).

[14] M. C. Rechtsman, J. M. Zeuner, Y. Plotnik, Y. Lumer, D. Podolsky, F. Dreisow, S. Nolte, M. Segev, and A. Szameit, Nature **496**, 196 (2013).

[15] J. Otterbach, M. Moos, D. Muth, and M. Fleischhauer, Phys. Rev. Lett. **111**, 113001 (2013).

[16] I. Carusotto and C. Ciuti, Rev. Mod. Phys. **85**, 299 (2013).

[17] K. L. Hur, L. Henriet, A. Petrescu, K. Plekhanov, G. Roux, and M. Schiró, Comptes Rendus Physique **17**, 808 (2016).

[18] C. Noh and D. G. Angelakis, Reports on Progress in Physics **80**, 016401 (2017).

[19] M. J. Hartmann, Journal of Optics **18**, 104005 (2016).

[20] M. Schiró, C. Joshi, M. Bordyuh, R. Fazio, J. Keeling, and H. E. Türeci, Phys. Rev. Lett. **116**, 143603 (2016).

[21] M. Fitzpatrick, N. M. Sundaresan, A. C. Y. Li, J. Koch, and A. A. Houck, Phys. Rev. X **7**, 011016 (2017).

[22] J. M. Fink, A. Dombi, A. Vukics, A. Wallraff, and P. Domokos, Phys. Rev. X **7**, 011012 (2017).

[23] A. A. Houck, H. E. Tureci, and J. Koch, Nature Physics **8** (2012).

[24] S. Schmidt and J. Koch, Annalen der Physik **525**, 395 (2013).

[25] I. Bloch, J. Dalibard, and S. Nascimbène, Nature Physics **8**, 267 EP (2012).

[26] J. G. Bohnet, B. C. Sawyer, J. W. Britton, M. L. Wall, A. M. Rey, M. Foss-Feig, and J. J. Bollinger, Science **352**, 1297 (2016).

[27] S. Diehl, A. Tomadin, A. Micheli, R. Fazio, and P. Zoller, Phys. Rev. Lett. **105**, 015702 (2010).

[28] L. M. Sieberer, S. D. Huber, E. Altman, and S. Diehl, Phys. Rev. Lett. **110**, 195301 (2013).

[29] T. E. Lee, S. Gopalakrishnan, and M. D. Lukin, Phys. Rev. Lett. **110**, 257204 (2013).

[30] J. Jin, D. Rossini, R. Fazio, M. Leib, and M. J. Hartmann, Phys. Rev. Lett. **110**, 163605 (2013).

[31] J. Marino and S. Diehl, Phys. Rev. Lett. **116**, 070407 (2016).

[32] O. Scarlatella, R. Fazio, and M. Schiró, Phys. Rev. B **99**, 064511 (2019).

[33] H.-P. Breuer and F. Petruccione, *The theory of open quantum systems*, 1st ed. (Oxford University Press, USA, 2002).

[34] T. E. Lee, H. Häffner, and M. C. Cross, Physical Review A **84**, 031402 (2011).

[35] J. Qian, G. Dong, L. Zhou, and W. Zhang, Physical Review A **85**, 065401 (2012).

[36] M. Marcuzzi, E. Levi, S. Diehl, J. P. Garrahan, and I. Lesanovsky, Physical review letters **113**, 210401 (2014).

[37] J. Jin, D. Rossini, R. Fazio, M. Leib, and M. J. Hartmann, Phys. Rev. Lett. **110**, 163605 (2013).

[38] J. Jin, D. Rossini, M. Leib, M. J. Hartmann, and R. Fazio, Physical Review A **90**, 023827 (2014).

[39] M. Foss-Feig, P. Niroula, J. T. Young, M. Hafezi, A. V. Gorshkov, R. M. Wilson, and M. F. Maghrebi, Physical Review A **95**, 043826 (2017).

[40] M. Biondi, G. Blatter, H. E. Türeci, and S. Schmidt, Physical Review A **96**, 043809 (2017).

[41] C.-K. Chan, T. E. Lee, and S. Gopalakrishnan, Physical Review A **91**, 051601 (2015).

[42] R. M. Wilson, K. W. Mahmud, A. Hu, A. V. Gorshkov, M. Hafezi, and M. Foss-Feig, Physical Review A **94**, 033801 (2016).

[43] H. Spohn, Letters in Mathematical Physics **2**, 33 (1977).

[44] F. Minganti, A. Biella, N. Bartolo, and C. Ciuti, Phys. Rev. A **98**, 042118 (2018).

[45] H. Weimer, Physical Review Letters **114**, 040402 (2015).

[46] M. Biondi, S. Lienhard, G. Blatter, H. E. Türeci, and S. Schmidt, New Journal of Physics **19**, 125016 (2017).

[47] J. Jin, A. Biella, O. Viyuela, L. Mazza, J. Keeling, R. Fazio, and D. Rossini, Phys. Rev. X **6**, 031011 (2016).

[48] A. J. Daley, Advances in Physics **63**, 77 (2014).

[49] T. Prosen and M. Žnidarič, J. Stat. Mech. **2009**, P02035 (2009).

[50] J. J. Mendoza-Arenas, S. R. Clark, S. Felicetti, G. Romero, E. Solano, D. G. Angelakis, and D. Jaksch, Phys. Rev. A **93**, 023821 (2016).

[51] F. Vicentini, F. Minganti, R. Rota, G. Orso, and C. Ciuti, Physical Review A **97**, 013853 (2018).

[52] J. Jin, A. Biella, O. Viyuela, C. Ciuti, R. Fazio, and D. Rossini, Phys. Rev. B **98**, 241108 (2018).

[53] A. Kshetrimayum, H. Weimer, and R. Orús, Nature Communications **8**, 1291 (2017).

[54] Z. Cai and T. Barthel, Physical review letters **111**, 150403 (2013).

[55] This is due to the fact that each site is coupled to the x and y components of the total magnetization of the $N-1$ other sites via J, and the fluctuations of this magnetization generically become small compared to its mean when $N \to \infty$. Neglecting these fluctuations gives a MF state with uncorrelated sites.

[56] E. Mascarenhas, H. Flayac, and V. Savona, Phys. Rev. A **92**, 022116 (2015).
[57] U. Schollwöck, Annals of Physics **326**, 96 (2011), january 2011 Special Issue.
[58] M. P. Zaletel, R. S. K. Mong, C. Karrasch, J. E. Moore, and F. Pollmann, Phys. Rev. B **91**, 165112 (2015).
[59] G. Benenti, G. Casati, T. Prosen, D. Rossini, and M. Žnidarič, Phys. Rev. B **80**, 035110 (2009).
[60] ITensor Library, http://itensor.org (version 2.1).
[61] K. Bidzhiev and G. Misguich, Phys. Rev. B **96**, 195117 (2017).
[62] H. Landa, M. Schiró, and G. Misguich, "In preparation,".
[63] E. Stoudenmire and S. R. White, Annu. Rev. Condens. Matter Phys. **3**, 111 (2012).
[64] D. Porras and J. I. Cirac, Phys. Rev. Lett. **92**, 207901 (2004).
[65] A. Friedenauer, H. Schmitz, J. T. Glueckert, D. Porras, and T. Schätz, Nature Physics **4**, 757 (2008).
[66] C. Schneider, D. Porras, and T. Schaetz, Reports on Progress in Physics **75**, 024401 (2012).
[67] R. Islam, C. Senko, W. Campbell, S. Korenblit, J. Smith, A. Lee, E. Edwards, C.-C. Wang, J. Freericks, and C. Monroe, Science **340**, 583 (2013).
[68] J. Smith, A. Lee, P. Richerme, B. Neyenhuis, P. W. Hess, P. Hauke, M. Heyl, D. A. Huse, and C. Monroe, Nature Physics **12**, 907 (2016).
[69] W. Casteels, R. Fazio, and C. Ciuti, Physical Review A **95**, 012128 (2017).